# Helium-Induced Weld Cracking in Low Heat Input GMA Weld Overlays

*Helium effects on fusion-zone porosity and HAZ cracking are minimized using a technique for shallow penetration welding*

BY S. H. GOODS AND C. W. KARFS

ABSTRACT. The influence of entrapped helium on weldability was examined for an AISI Type 304 stainless steel. Two types of welding processes were compared: conventional, deep penetration, gas metal arc stringer bead welding, and a novel, very shallow penetration gas metal arc weld overlay process. Helium concentrations ranging between 2.7 and 85.0 atomic parts per million were generated in test specimens by tritium charging them to saturation and then allowing the dissolved tritium to decay to $^3$He. Detailed scanning electron microscopy subsequent to welding revealed the presence of cracking in the heat-affected zone of all samples, including the lowest heat input weld overlays. No such cracking was observed in helium-free control specimens. In every instance, the cracking in the helium-bearing specimens was intergranular. The grain boundary facets of these intergranular cracks were decorated with a uniform distribution of dimples similar to that typically associated with high-temperature gas bubble embrittlement. While all of the helium-bearing specimens exhibited some amount of cracking (as measured by crack length, location and total number of cracks), the extent of cracking was significantly reduced in the shallow penetration overlays vs. the stringer bead welds.

## Introduction

The exposure of metallic materials, such as structural components of the first wall and blanket of a fusion reactor, to neutron irradiation will induce changes in both the material composition and microstructure. Along with these changes can come a corresponding deterioration in corrosion resistance and mechanical properties. It is not unreasonable, therefore, to expect that the repair and replacement of degraded reactor components will be necessary. Even in current nuclear reactors, the repair of defects such as stress corrosion cracks in reactor tanks may eventuate (Ref. 1). Such repairs may require the joining of irradiated materials through the use of fusion welding procedures.

Fusion welding processes will be among the preferred techniques for repairing flaws in these irradiated reactor materials. This preference is derived from 1) its amenability to remote execution in hostile and nearly inaccessible reactor core environments, 2) its ASME (American Society of Mechanical Engineering) code recognition and qualification, 3) the prospect of fabricating an actual load-carrying structural repair (rather than simply a superficial covering of a crack), 4) the chemical and radiation compatibility of the repair material with the reactor, and 5) the inspectability of the repair. Indeed, such fusion welding repairs have already been attempted using conventional gas tungsten arc (GTA) welding processes (Ref. 1).

The repair of irradiated structures using such welding practices will be made exceedingly difficult because the irradiated reactor steels contain entrapped helium, which is formed by neutron reactions with alloy constituents, principally, with boron as:

$$^{10}B + n \rightarrow {}^7Li + {}^4He$$

and with nickel as:

$$^{58}Ni + n \rightarrow {}^{59}Ni + \gamma$$

$$^{59}Ni + n \rightarrow {}^{56}Fe + {}^4He$$

The very low solubility of helium in metals results in its tendency to form small clusters on the order of a few tenths of nanometers in diameter at low temperatures (<100°–200°C/212°–392°F) or 2–10 nanometer-sized bubbles at higher temperatures (<600°C/1112°F). Preferred nucleation sites for this helium-induced damage are lattice inhomogeneities such as radiation-induced defects, precipitate interfaces, dislocations, and, most importantly, grain boundaries. At elevated temperatures, these clusters and bubbles grow very rapidly and under applied stress can severely weaken grain boundaries. Because conventional, deep penetration, fusion welding processes produce high stresses (above the yield strength) as well as high temperatures (above the melting point), entrapped helium can severely affect the weldability and postweld properties of irradiated materials. The severity of the observed effects is thought to be dominated by helium content and by the extent and magnitude of the temperature and stress fields that prevail near the fusion line during welding. In fact, an attempt to repair a leaking crack in an irradiated portion of a reactor using conventional deep penetration gas tungsten arc (GTA) welding practices was unsuccessful (Ref. 2). The failure was manifested in the formation of an extensive, interconnected network of intergranular cracks in the heat-affected zone (HAZ) and led to the abandonment of the entire reactor.

Other work has further demonstrated that such conventional welding techniques cannot be used with materials bearing helium at modest concentrations (2–150 atomic parts per million). In one such experiment, the propensity for weld cracking was examined in 316 stainless steel as a function of helium content (Ref. 3). Here, unlike irradiated material, the helium was

**KEY WORDS**

He-Induced Cracking
GMAW
GMAW Overlays
Austenitic Stainless
Fusion-Zone Porosity
HAZ Cracking
Weld Heat Input
Weldability
Microstructure
Intergranular Cracks

*S. H. GOODS and C. W. KARFS are with the Engineering Materials Division, Sandia National Laboratories, Livermore, Calif.*

**Table 1—Composition (wt-%)**

| Material | Cr | Ni | C | Mn | Mo | Cu | Si | S | P | Fe |
|---|---|---|---|---|---|---|---|---|---|---|
| 304 | 18.22 | 8.28 | 0.073 | 1.39 | — | — | 0.52 | 0.016 | 0.023 | Bal |
| 308L | 20.4 | 10.0 | 0.015 | 2.0 | 0.23 | 0.09 | 0.36 | 0.017 | 0.026 | Bal |

introduced into the test specimens through tritium charging and aging (the dissolved tritium subsequently decays to $^3$He). Full-penetration GTA welds were fabricated on fully constrained, helium-bearing plates after the remaining tritium was vacuum extracted. The results of this study illustrated the significant effects that helium can have on the weldability of a material. At helium concentrations as low as 2.3 atomic parts per million (appm), catastrophic cracking was observed in the heat-affected zone of welded plates. The cracking was exclusively intergranular and occurred in regions where the stress and temperature were most conducive to grain boundary cavity growth, which were not necessarily in the hottest regions of the weldment.

The morphology of these cracks exhibited the characteristic features of high-temperature helium embrittlement. At high magnification, these intergranular facets were found to be decorated with a distribution of very small dimples which originated from the initial distribution of helium gas bubbles. Transmission electron microscopy revealed that the observed degradation in weldability and catastrophic cracking resulted solely from the growth and coalescence of the grain boundary helium gas bubble microstructure. Mechanical properties from uncracked portions of these weldments were also assessed as part of this study. Even in the absence of gross cracking, the residual ductility of welds was severely reduced because of the presence of helium.

The difficulties in fabricating conventional GTA welds on helium-bearing materials has lead to the development of a novel, shallow penetration, weld overlay process.[1] In this process, a 0.6- to 1.5-mm (0.02 to 0.06-in.) thick gas metal arc (GMA) "pad" of filler metal is welded onto the helium-bearing workpiece. The fusion boundary penetrates only 0.1 to 0.2 mm (0.004 to 0.008 in.) into the underlying metal. In principle, the volume of material that experiences high temperatures and the area potentially affected by helium is restricted to a much more narrow region beneath the weld than that which would be associated with a conventional, deep penetration weld. This report summarizes the findings of the characterization of these welds' microstructures.

## Experimental Procedure

### Materials and Tritium Charging Conditions

Specimens for welding were fabricated from 304 stainless steel. These specimens were rectangular, having the dimensions: 120.6 mm long × 31.8 mm wide × 6.4 mm high (4.75 × 1.25 × 0.25 in.). The composition of the steel is shown in Table 1.

The as-received material had been solution annealed at 1040°C (1904°F) and fast cooled in air. The yield strength at room temperature was 250 MPa (36 ksi), the ultimate tensile strength was 580 MPa (84 ksi) and the total elongation was 68%.

The plates were then tritium charged and aged in order to generate trapped helium over a range of concentrations between ≈3 appm and ≈85 appm (tritium undergoes the decay reaction $^3_1H \rightarrow {}^3_2He + \beta$, and has a 12.3-year half-life). All specimens were charged at 400°C (752°F) for 30 days. At the end of that time, the charging vessels were cooled to ambient temperature over a period of approximately 10 hours. The diffusion of tritium is sufficiently rapid at 400°C to ensure its uniform distribution through the cross-section of the specimen (Ref. 4). In order to generate the desired range of concentration, two separate charging runs, each at a different tritium overpressure, were performed. A low-pressure charging run performed at 4.1 MPa (0.6 ksi) resulted in a helium build-in rate of approximately 3 appm/month, while a high-pressure run performed at 63.5 MPa (9.2 ksi) yielded a helium build-in rate of ≈15 appm/month. At the end of the 30-day charging period, several specimens from each charging vessel were immediately vacuum offgassed at 450°C (842°F) for 5 days to extract the tritium and stop the further build-in of helium. Helium is easily trapped in a metal. Therefore, it does not undergo long-range diffusion and unlike the tritium does not offgas during vacuum annealing.

The remaining specimens were stored at −40°C (−40°F) to continue aging in helium. At this temperature, tritium is essentially immobile in stainless steel. Thus, the uniform distribution established during the high-temperature charging was maintained throughout the aging period. When the helium levels had increased to the desired values, additional specimens were subsequently removed from storage and offgassed at the same temperature and for the same time as previously indicated.

### Welding

Welding was performed on plates having helium concentrations of 2.7, 9.4, 16.6 and 85.0 appm. Two types of GMA welds

*(1) This welding process was developed by E.A. Franco-Ferreira at Westinghouse Savannah River Company, Aiken, S.C., to whom the reader is referred for details of the procedure.*

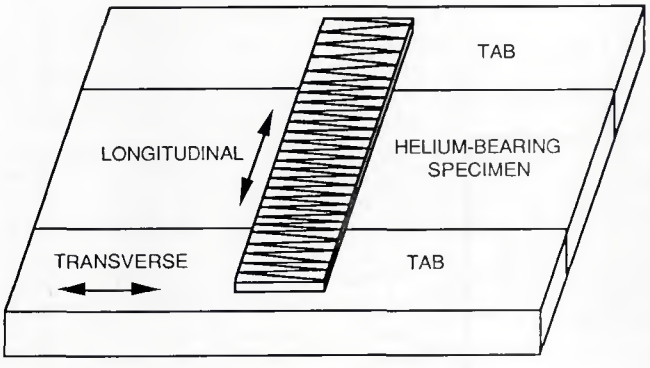


*Fig. 1—Schematic representation of weld overlay. Transverse and longitudinal directions are defined as shown.*

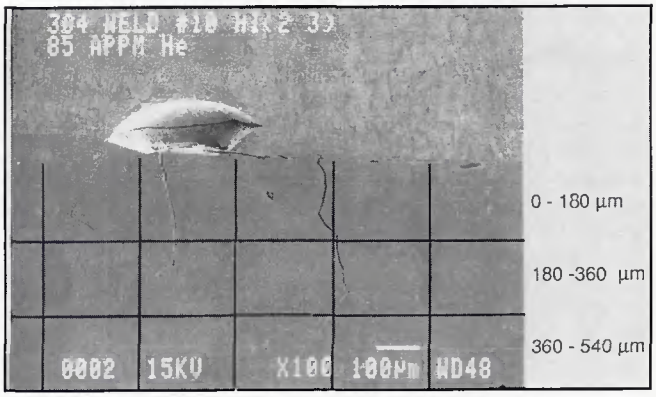


*Fig. 2—Crack profiling procedure involved dividing the heat-affected zone into equal areas. The number and length of cracks in each area was then recorded. The large, lens-shaped feature in the fusion zone is a welding defect unrelated to the presence of helium in the workpiece.*

were fabricated: conventional stringer bead welds that had relatively deep penetrations (on the order of several millimeters) into the underlying workpiece, and shallow penetration GMA weld overlays. The composition of the 308L welding wire is shown in Table 1. The overlay procedure consisted of oscillating a consumable electrode so that a 25-mm (1-in.) wide pad of weld metal was fabricated in a weave pattern as shown schematically in Fig. 1. The helium-bearing test plates were placed between start and stop tabs. In the analysis that follows, "transverse" sections refer to cuts made parallel to the actual weld bead. The thickness of the pad was approximately 1.5 mm (0.06 in.). This overlay process resulted in minimal penetration into the underlying workpiece (0.1 to 0.2 mm) and is intended to minimize the volume of material beneath the weld that is heated to high temperatures. In the same manner, the shrinkage stresses generated by the overlay are considerably different than those established by the more conventional process. Three welds were examined on each plate: one stringer bead weld and two overlays with different average heat inputs. The weld parameters are given in Table 2.

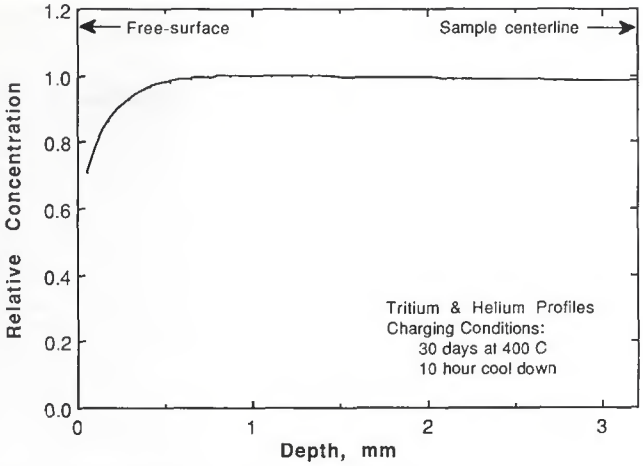


*Fig. 3—Normalized distribution of tritium and helium in a charged and aged specimen. Near surface gradients result from offgassing during cooling from the elevated charging temperature.*

### Metallography

Sections of weldments were cut from the welded plates for analysis. Detailed metallography was performed on the plates containing He at all four concentrations. All metallography was done on sections cut parallel to the weld approximately 6 mm (0.24 in.) from the interface between the start tab and the specimen.

Specimens were also cut along the longitudinal midline so that approximately 12 mm (0.47 in.) of weld interface and heat-affected zone beneath the weld could be examined. These sections were mounted, ground and polished to a 0.25 $\mu$m finish using conventional metallographic procedures. In order to preserve the fine structure of the intergranular cracking, a final etch-polish procedure was used. This procedure consisted of polishing the specimens on cloth using a solution of 55 mL LECO Silica™, 4 mL $H_2O_2$ (3%) and 5 mL of an etch-polish solution (95 mL $H_2O$, 3 mL HCl and 2 mL $HNO_3$). After this final polish, the specimens were swab etched for 2 minutes using a solution comprised of equal parts HCl, $HNO_3$ and $CH_3COOH$. The specimens were then carbon coated. All metallography was done using electron microscopy.

### Crack Profiling

To meaningfully compare the extent of cracking between weldments, a protocol was established to count the number, length and location of cracks beneath the fusion line. Figure 2 is a low-magnification scanning electron micrograph of an overlay and illustrates the method used. The region extending to a depth of 540 $\mu$m beneath the fusion line was examined. This region was divided into three bands each having a depth of 180 $\mu$m. Each band was further partitioned into a number of rectangular elements as shown. The number of cracks present in each element of the grid was counted and their lengths were noted. In many cases, grain boundaries were extensively decorated with pores or cavities. For the purposes of this analysis, a crack was defined as any length of grain boundary in which more than 50% of the interface had clearly separated. Any grain boundary separation of $<10$ $\mu$m was ignored. If a crack extended beyond a single element or band, its total length was measured. However, its origin was assigned to the first band beneath the fusion line in which it appeared. Crack lengths were sorted into bins of: 10–50 $\mu$m, 50–100 $\mu$m, 100–200 $\mu$m, 200–500 $\mu$m and $>500$ $\mu$m. In addition to characterizing the extent of intergranular cracking in the HAZ, the weld interface was examined for other discontinuities such as the total length of nonfusion along the fusion line and the degree of porosity in the fusion-zone.

## Results

### Tritium and Helium Profiles

The final tritium profile after the 30-day charging period is shown in Fig. 3. This

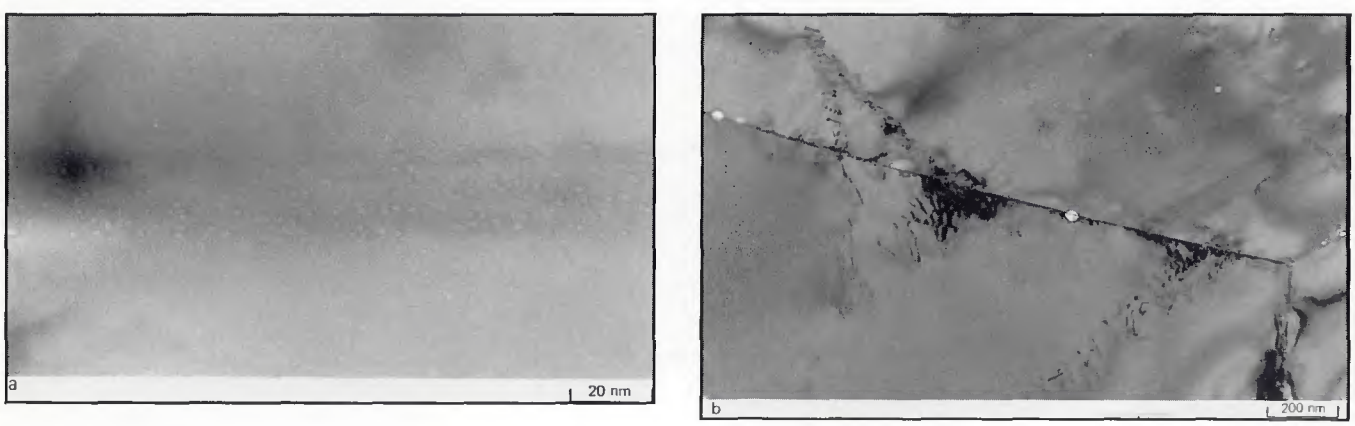


*Fig. 4—Helium bubble microstructure in tritium charged and aged specimen. A—After offgassing at 450°C (852°F) stainless steel; B—after annealing at 850°C (1562°F), the bubble morphology has coarsened, resulting in larger and more widely spaced bubbles.*

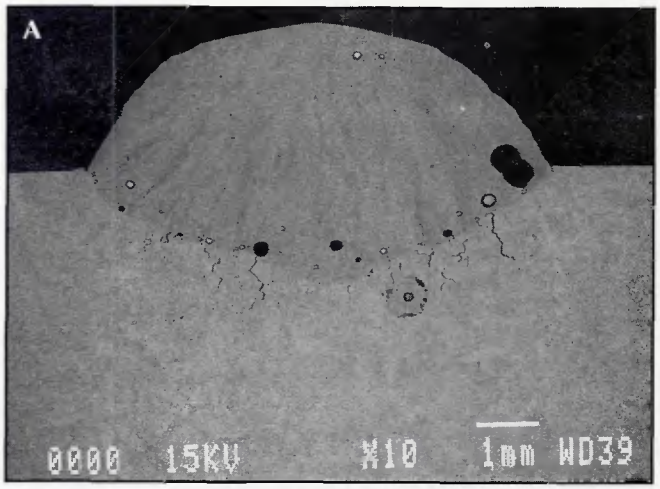


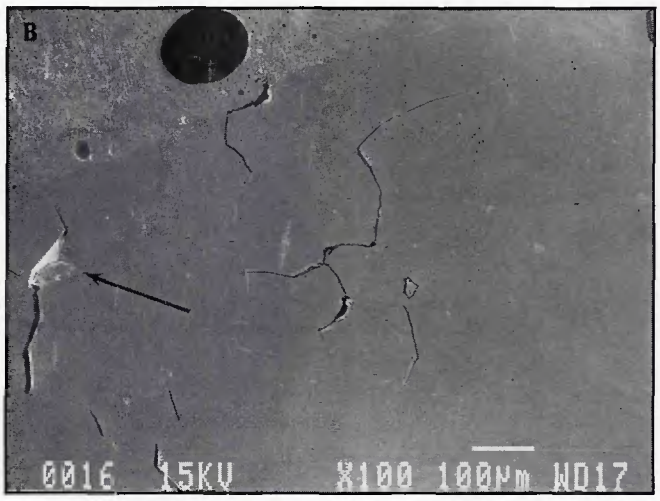


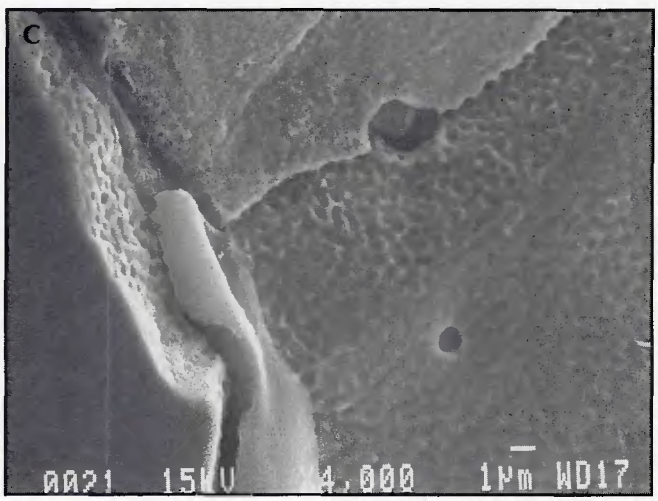


*Fig. 5—Porosity and cracking in stringer bead specimen. A—Large pores within the weld metal decorate the fusion boundary; B—HAZ cracking is intergranular. Arrow identifies grain boundaries exposed by a missing grain; C—grain boundary facets are decorated with a uniform distribution of dimples. (85.0 appm He, heat input = 60.8 J/mm²)*

distribution was calculated using DIFFUSE (Ref. 5), a one-dimensional diffusion code that takes into account time-temperature-pressure history and specimen geometry. For a radioactively unstable isotope, such as tritium, the code can also predict the distribution of daughter products ($^3$He, in the present case). Figure 3 shows the specimen surface-to-centerline concentration normalized so that the peak value equals one. The code predicts that the tritium concentration within the interior of the specimen is nearly constant. There is a near surface, tritium depleted region. This results from tritium offgassing during the cool-down of the pressure vessel from 400°C to ambient temperature.

Since the resulting helium distribution is a direct function of the tritium profile (integrated over time), the through-thickness distribution of helium in an aged specimen is essentially identical to that shown for tritium in Fig. 3. Thus, the shallow penetration weld overlays were fabricated into regions exhibiting some variation in helium concentration. Depending on the actual depth of the fusion line, the helium concentration was never less than 80% of the maximum. For the sake of simplicity, the helium levels reported reflect the bulk concentration, rather than the local, near surface value.

**Table 2—Welding Parameters**

| Type | Current (I) | Voltage (V) | Travel[a] mm/s (in./min) | Oscil[b] mm/s (in./min) | Width[c] mm (in.) | Heat input[d] J/mm² (kJ/in.²) |
|---|---|---|---|---|---|---|
| Stringer | 150 | 26.5 | 6.77 (16.0) | 0 | 8.38 (0.33) | 60.8 (39.2) |
| Overlay #1 | 80 | 19.5 | 1.02 (2.4) | 17.1 (40.5) | 25.4 (1.0) | 60.5 (39) |
| Overlay #2 | 45 | 19.5 | 0.64 (1.5) | 17.1 (40.5) | 25.4 (1.0) | 54.4 (35.1) |

(a) Travel refers to the velocity of the electrode in the longitudinal direction.
(b) Oscillation refers to the velocity of the electrode in the transverse direction.
(c) Width is defined as the length of the fusion line.
(d) For the overlays, heat input is calculated as Efficiency × (I × V)/(Travel × width). It is further modified by the overlap of the weave pattern. Some of these factors, including process efficiency and degree of overlap, are poorly known. In the table, efficiency is taken as 1.0. Thus, the tabulated values should be used for comparative purposes only.

While Fig. 3 illustrates the macroscopic distribution of helium within a specimen, it is well known that the offgassing procedure used results in a local partitioning of helium to grain boundaries and other microstructural features in the form of a gas bubble microstructure (Refs. 6, 7). The size and spacing of the gas bubbles depend in a complex way on a number of parameters, including grain boundary structure, annealing temperature, time at temperature and helium concentration. Figure 4A is a transmission electron micrograph that shows the typical bubble microstructure developed in a 316L stainless steel specimen following the charging, aging and offgassing procedure. In this specimen, the helium concentration was 33 appm. The micrograph reveals a well-defined grain boundary bubble microstructure. The bubbles lying along the grain boundaries are very small (2–3 nm). The bubbles are also very closely spaced. Comparable bubble microstructures were observed in the specimens used in the present study. In addition to this grain boundary structure, helium bubbles were present within the grains, primarily at dislocations and stacking faults.

Such bubble microstructures are not

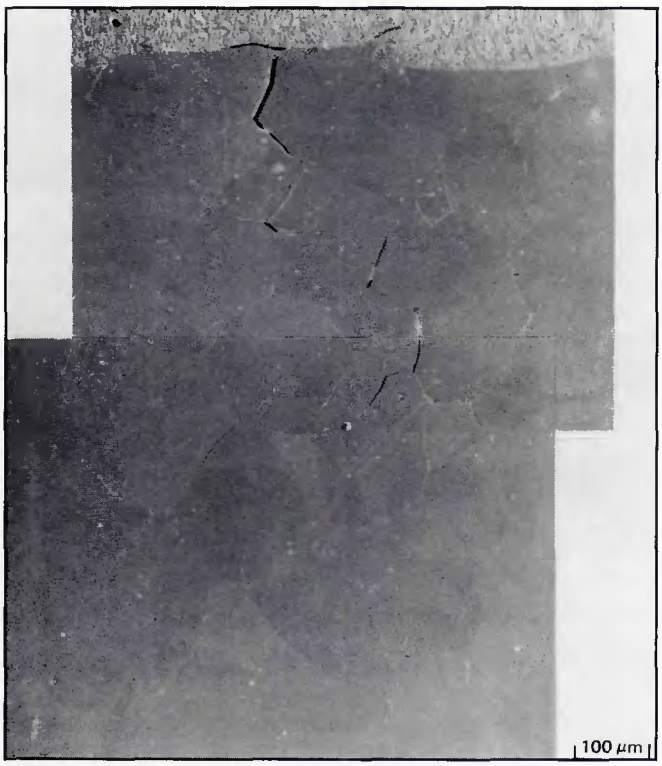


*Fig. 6 — Scanning electron micrograph showing transverse section below weld overlay. A nearly continuous network of cracking is present in the HAZ. (85.0 appm He, heat input = 60.5 J/mm²)*

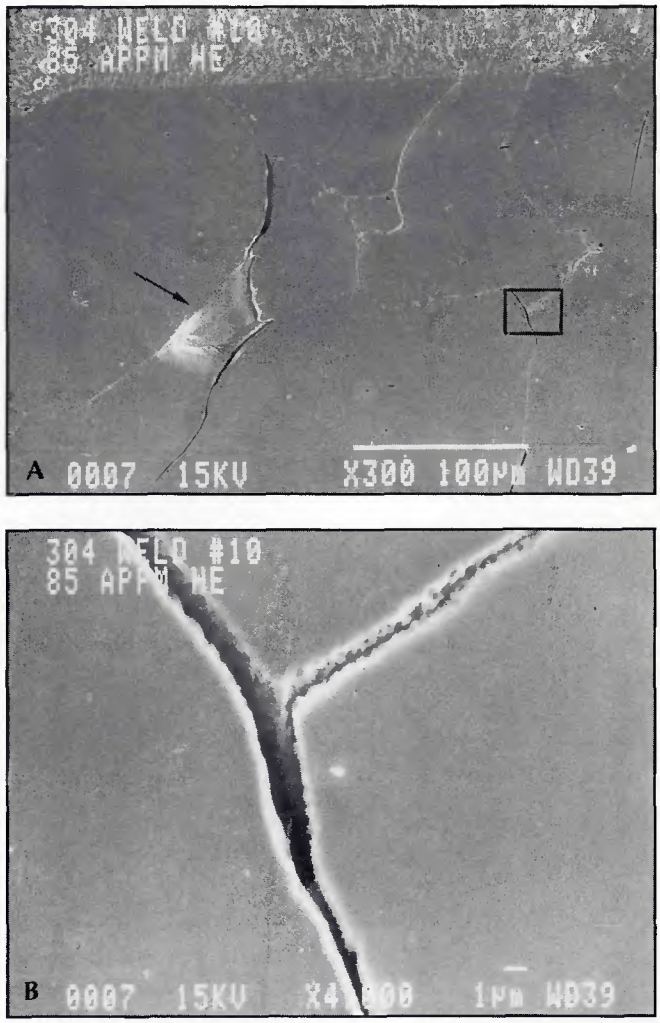


*Fig. 7 — A — High-magnification micrograph reveals intergranular nature of HAZ cracking; B — at higher magnification of highlighted region in Fig. 7A, intergranular facets reveals dimple structure. (Overlay, 85.0 appm He, heat input = 60.5 J/mm²)*

stable. Rather, they tend to coarsen with increasing annealing or offgassing temperature. An example of this is shown in the transmission electron micrograph — Fig. 4B. The figure shows the resulting microstructure in the same 316L stainless steel specimen that was tritium charged and offgassed in a manner identical to that shown in Fig. 4A. However, it was subjected to further vacuum annealing at 850°C (1562°F). The bubbles are now much larger (30–40 nm diameter) and much more widely spaced (0.5–1.0 μm).

#### Metallography

*Stringer beads.* Figure 5 is a metallographic cross-section of the highest heat input stringer bead weld, 60.8 J/mm². The figure reveals that helium had a profound effect on the weldability of 304 stainless steel. For the specimen shown here (85.0 appm He), the micrograph (Fig. 5A) reveals that there was a large amount of porosity within the fusion zone, arising from the mixing of the molten 308L welding wire and helium-bearing 304 base metal prior to solidification. Similar fusion-zone porosity has been observed in GTA welded 316 stainless steel (Ref. 3). Figure 5 also reveals that in the HAZ, cracking was found to extend at least 1 mm (0.04 in.) below the fusion line. At higher magnification (Fig. 5B), it can be clearly seen that this cracking was intergranular. The arrow in Fig. 5B highlights an area where cracking was so severe that a grain has separated from the remaining specimen. At still higher magnification (Fig. 5C), the grain boundary facets exposed by the separation of the grain reveal a characteristic dimple structure associated with high-temperature helium embrittlement. The dimple spacing is on the order of 0.5 to 1.0 μm. Even at the lowest helium content studied (2.7 appm), cracking in the HAZ beneath these high heat input stringer bead welds was significant — a nearly continuous network of cracks was seen to extend well over 200 μm below the fusion line. No such fusion-zone porosity or HAZ cracking was observed in helium-free control specimens.

*Overlays.* The weld overlays were free of the large porosity shown in Fig. 5. This can be understood in terms of the minimal penetration of the weld into the workpiece which, in turn, resulted in much less mixing of helium-bearing metal into the molten pool. Further, the overlay welding induced less extensive cracking than was the case for the stringer bead welds in specimens of comparable helium content. This was most likely due to the less extensive shrinkage stresses associated with the shallow penetration. Figure 6 shows a typical transverse cross-section beneath the weld overlay of a specimen containing 85 appm helium. The overlay was fabricated using the welding parameters resulting in the higher of the two net heat inputs, 60.5 J/mm². At the top of the figure, the fusion line clearly delineates the resolidified weld metal from the HAZ. Within the HAZ, extensive cracking was apparent, although, to a far lesser extent, that was the case for the conventional weld shown in Fig. 5. Here, as in all of the

helium-bearing specimens, the cracking was intergranular and was preferentially oriented normal to the overlay fusion boundary. The furthermost extent of cracking shown in Fig. 6 is ≈600 μm beneath the fusion line. It can also be seen that the crack faces can be separated by as much as 10 μm. These wide separations resulted from thermal stress-induced deformation of the HAZ as the weld cooled from high temperature (Ref. 8). As before, no such cracking was observed in helium-free control specimens.

Another type of discontinuity can be seen in Fig. 6. These are roughly spherical pores that lie within the grain matrix. These features are present in both the charged and aged (helium-bearing) as well as in the uncharged, helium-free specimens. They arise from the dissolution of inclusions during metallographic preparation and are unrelated to helium or welding effects.

Figure 7 shows additional cracking in the same specimen containing 85 appm He. As in the previous figure, the predominant cracking is oriented nearly normal to the fusion line. At the higher magnification of Fig. 7A, the intergranular nature of the cracking is more clearly revealed. Indeed, the arrow indicates an entire exposed grain boundary facet oriented nearly parallel to the plane of the micrograph. The highlighted area in Fig. 7A is shown at yet higher magnification in Fig. 7B. At this magnification, the grain boundary facets are revealed to be decorated with a dimple structure similar to that shown in Fig. 5.

As before, the dimple spacing is exceedingly uniform, approximately 0.5 to 1.0 μm, and is characteristic of high-temperature helium embrittlement. The uniformity of the dimple spacing suggests that the dimples formed from the preexisting bubble microstructure. That the spacing of the dimples is greater than the helium bubble spacing shown in Fig. 4A further suggests that the bubbles agglomerate during the early stages of welding to form a coarser structure (*i.e.*, during the preheating of the workpiece as the electrode approaches any given point in the path of the weld) or afterward, during the initial cooldown. It is from this coarsened helium bubble microstructure, much like that shown in Fig. 4B, that the dimple structure arises. Similar dimple structures have been observed on intergranular cracks in gas tungsten arc welded 316 stainless steel containing helium at concentrations between 2.3 and 256 appm helium (Ref. 3) and within the HAZ of weldments of irradiated stainless steel containing ≈3 appm He (Ref. 9). Similar cracking was observed in all of the tritium-charged and aged specimens. For the overlays, the extent of the damage occurred to a greater or lesser degree depending on helium content and heat input, as will be described in the next section. In every instance, the cracking characteris-

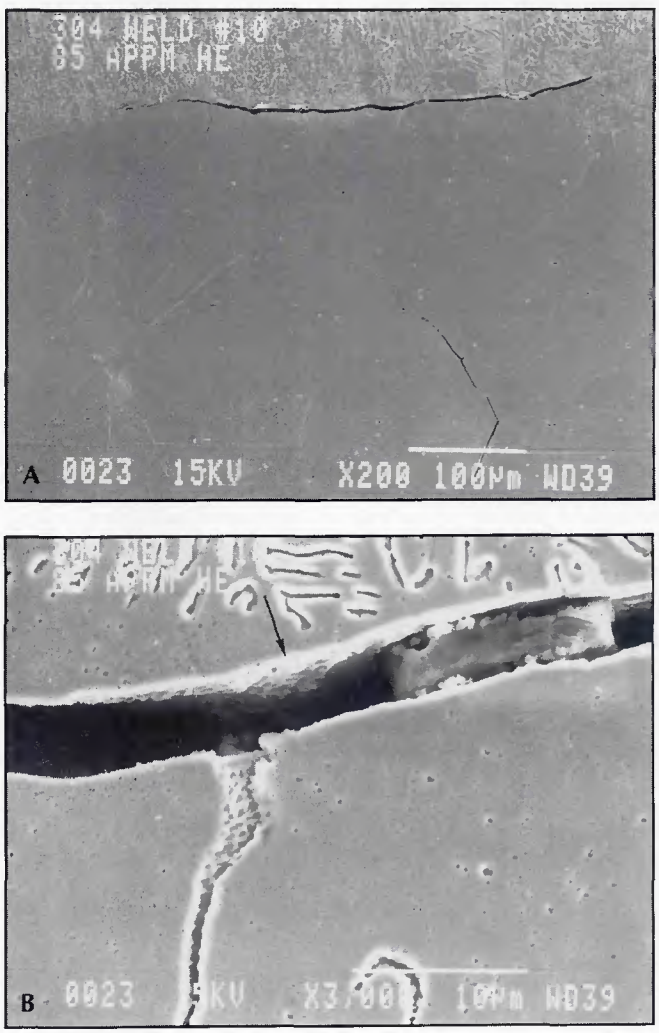


*Fig. 8 — Nonfusion in a helium-bearing specimen; B — higher magnification of highlighted region in Fig. 8A reveals dimple structure similar to that on grain boundary facets. (Overlay, 85.0 appm He, heat input = 60.5 J/mm²)*

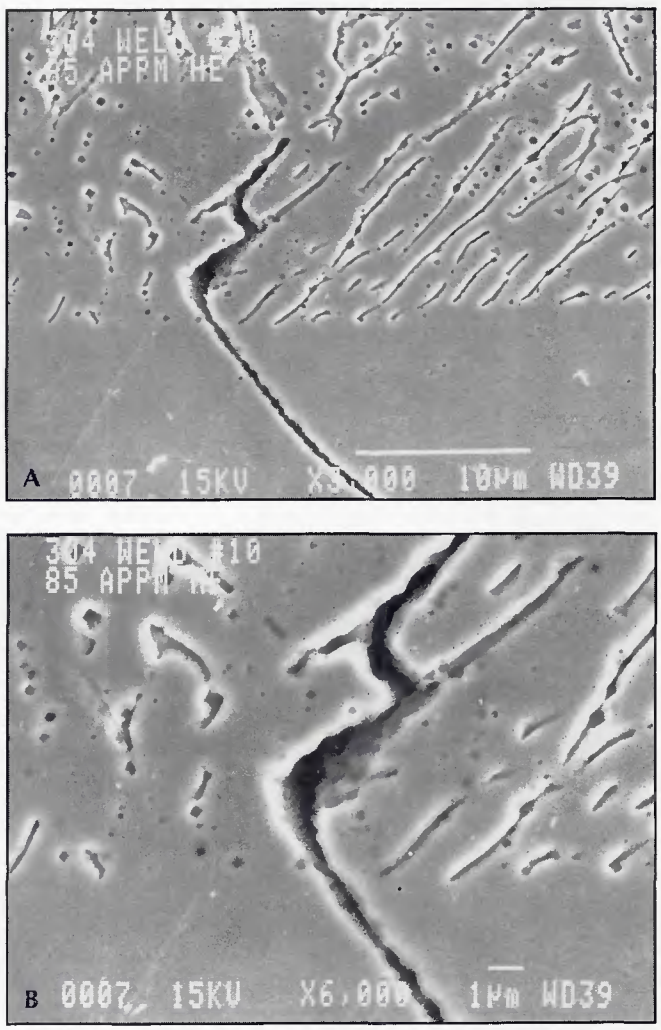


*Fig. 9 — Cracking extends into fusion zone in helium-bearing specimen; B — intertacial cracks are decorated with dimple structure similar to that on grain boundary facets. (Overlay, 85.0 appm He, heat input = 60.5 J/mm²)*

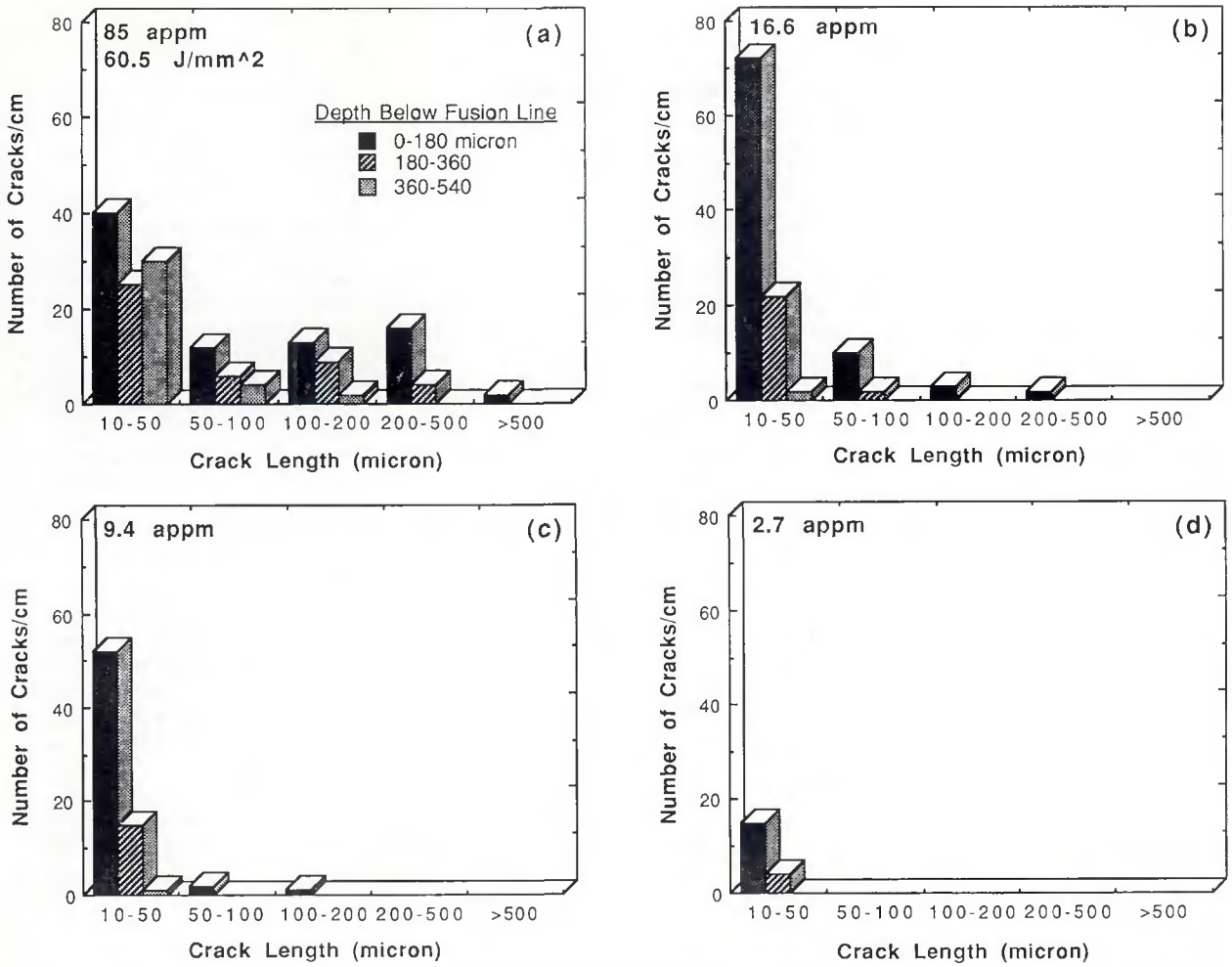


*Fig. 10—Distribution of cracks in the HAZ of the high heat input weld overlays for all helium-bearing specimens. (Heat input = 60.5 J/mm²)*

tics were identical to those described in the previous paragraphs, *i.e.*, intergranular with the grain boundary facets exhibiting a uniform dimple structure. In no instance were any toe cracks found that terminated at the specimen surface.

Figure 6 also reveals the presence of areas of nonfusion; that is, areas where the weld metal did not adhere to the underlying HAZ. Such areas are features that may be induced by helium and should be distinguished from incomplete fusion that is associated with weld wire feed and lack of melting. An example of this is clearly seen in Fig. 8A where a large fraction of the weld overlay has separated from the specimen. No such discontinuities were observed subsequent to welding in the unaged, helium-free specimens. Thus, as with the intergranular cracking, the observation of nonfusion was associated with the presence of helium. The arrow in Fig. 8B points to a region where the weld metal side of the nonfused fusion line exhibited the same kind of dimple structure as that described above for the intergranular cracks in the heat-affected zone, suggesting a similar cracking mechanism.

Cracking was found to extend beyond the HAZ and fusion line into the weld overlay itself. An example of this is shown in Fig. 9. However, the depth of cracking never extended more than approximately 10 $\mu$m into the overlay. The crack path in the weld metal is similar to that within the heat-affected zone in that the cracks follow the interfaces within the cast microstructures of the overlays. Similar interfacial cracking has been reported after welding high helium content 316 stainless steel (Ref. 3). Figure 9B reveals that the cracking in the fusion zone exhibited the same kind of dimple structure as that found in the heat-affected zone, again suggesting a similar helium-induced effect.

### Crack Profiling

Using the protocol described previously, the distribution of cracks within the weld heat-affected zones was determined for both the weld overlays and the stringer bead welds. Figure 10A shows the results of crack counting procedure (per cm of fusion line) for the high heat input weld overlay (60.5 J/mm²) in the highest helium content specimen. Over 130 cracks per centimeter of fusion line were counted in this specimen. More than 50% of these cracks were short, less than 50 $\mu$m in length. The origin of these cracks was not strongly dependent on their location with respect to the depth below the fusion line. In addition to these short cracks, there were a significant number of longer cracks. The longest crack measured was 680 $\mu$m in length. Most of these long cracks tended to originate immediately below the fusion line.

Figure 10B-D shows that the total number and length of cracks decreased dramatically with decreasing helium concentration. For the specimen containing 16.6 appm He (Fig. 10B), fewer than 100 cracks of all lengths were counted. Nearly 85% of these cracks were in the 10 to 50 $\mu$m range and approximately 80% of all the cracks, regardless of length, had their origin immediately below the fusion line. At 9.4 appm He, there were no cracks over 200 $\mu$m in length. At the lowest helium level, no cracks over 50 $\mu$m were found, and all cracks had their origin immediately below the fusion line. In a similar way, Fig. 11 summarizes the crack length observa-

tions for the lower heat input weld overlays across all helium concentrations. As with the previous figure, it is clear the propensity for cracking was substantially reduced with decreasing helium concentration. Indeed, at the lowest helium concentration, only one crack (<50 μm) was observed in the heat-affected zone beneath the weld.

Comparing Figs. 10 and 11 reveals that heat input is an important parameter in regard to the degree of cracking that resulted from applying the weld overlays, especially at low-He concentration. Even the relatively small decrease in heat input had a significant effect on the degree of cracking. The relationship between heat input, helium concentration and HAZ cracking can be seen in a more straightforward way in Fig. 12, where the total crack length is shown vs. helium concentration. For this figure, total crack length is approximated from the data presented in Figs. 10 and 11 by summing the number of cracks in each bin times the average bin length. The weld overlay data are represented by the solid lines, while the stringer bead welds are represented by the broken line. It is clear from this figure that the extent of cracking increased with increasing helium concentration. Although the data are limited, the figure indicates that the propensity for weld induced cracking in the shallow penetration overlays was reduced by decreasing heat input. However, it further shows that the welding process was an even more important factor in regard to cracking. While the heat input value for the deep penetration stringer bead welds were comparable to that for the highest heat input overlay, they exhibited significantly more HAZ cracking.

For the high heat input weld overlays, nonfusion accounted for 32% of the total fusion line in the highest helium content specimen. In the specimen containing 16.6 appm, it amounted to about 8%. At 9.4 appm helium, the total length of nonfused fusion line was negligible, less than 100 μm. Nonfused areas were not observed in the lowest helium content specimen. Nonfusion was not observed in any of the deep penetration stringer bead welds.

## Discussion

The metallographic results and crack counting protocol reveal that the degradation in weldability was extremely sensitive to helium concentration, the specific welding process and heat input. The role of helium in inducing cracking in the heat-affected zone of the welds was identical to that briefly described in the introduction. As a result of the thermal and mechanical response of the workpiece to the welding processes, the helium bubbles that resided at the grain boundaries grew and coalesced. Indeed, it was the coalescence of these relatively uniform arrays of grain boundary bubbles that gave rise to the characteristic dimple structure of the intergranular crack facets in the HAZ.

The mechanism of such cavity growth processes under high-temperature isothermal and isostatic (creep) conditions has been modeled extensively (Refs. 10–14) and experimentally examined in the literature (Refs. 15–18). The evidence presented in these studies strongly suggests that preexisting intergranular cavities (or helium bubbles) grow by a grain boundary/surface-self diffusion process, by the deformation (creep) of the matrix immediately surrounding the cavities, or by a combination of the two. In all cases, cav-

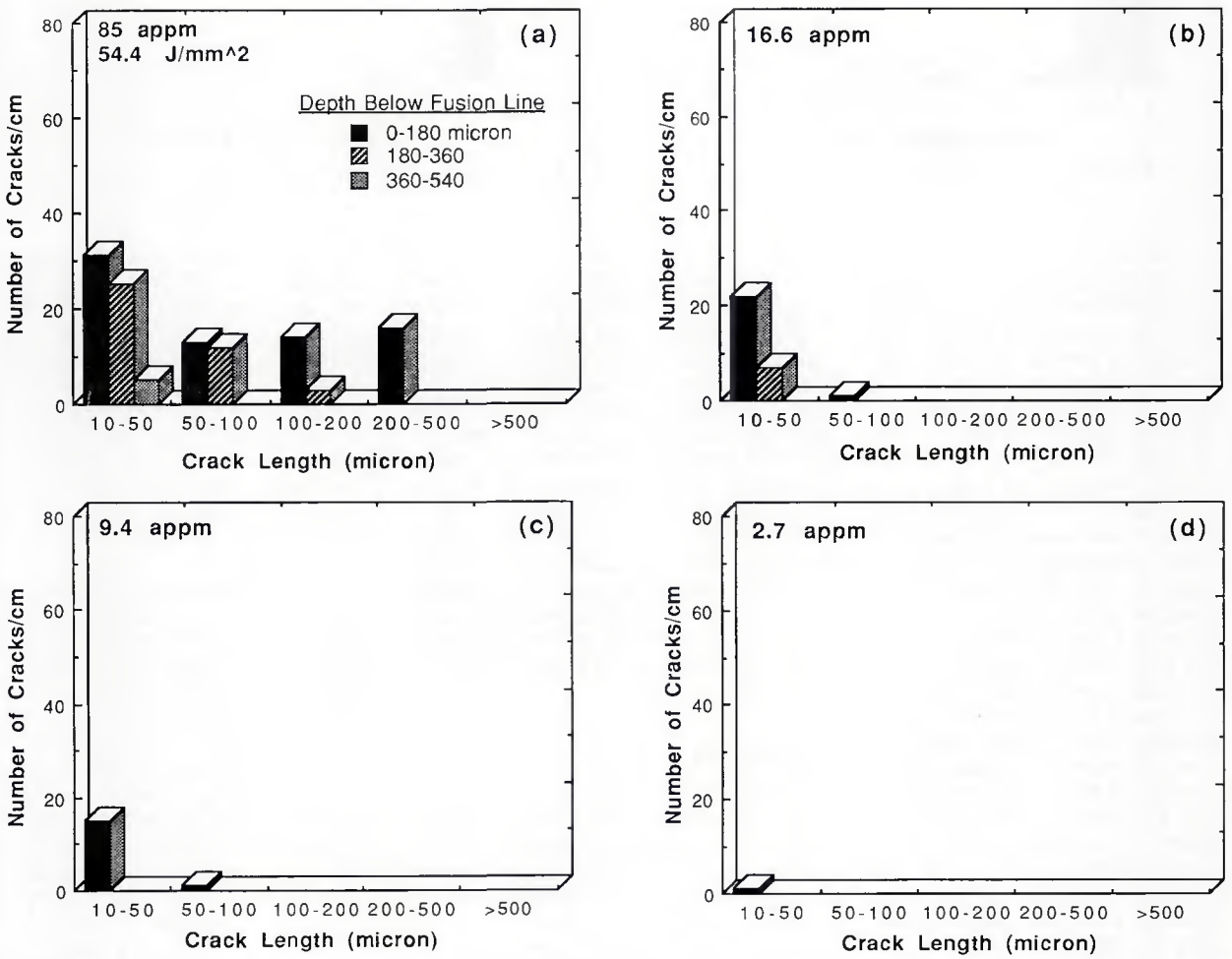


*Fig. 11—Distribution of cracks in the HAZ of the low heat input weld overlays for all helium-bearing specimens. (heat input = 54.4 J/mm²)*

ity growth is driven by tractions imposed on the precavitated grain boundary and fracture is therefore localized to the boundary. Thus, these preexisting cavity microstructures result in: 1) changes in fracture mode to one that is entirely intergranular in nature and 2) dramatically reduced ductility. Such embrittlement processes are usually observed at high temperature, near and above the half-melting point of a material where creep processes are rapid or where the vacancy concentration and mobility are adequate to sustain the growth mechanism. In these cases, the helium (or any inert, gaseous specie) itself, plays essentially no direct role in reducing high-temperature ductility. Rather, it acts only as a source for cavity nucleation prior to the imposition of temperature and stress.

In the present case, welding induced neither time independent temperatures nor stresses as addressed in these earlier studies. However, the degradation in weldability of the helium-bearing specimens examined here has its origins in precisely the same cavity growth mechanism as that just described. The role of the entrapped helium was to establish a preexisting, grain boundary bubble or cavity microstructure. These bubbles then grew and linked to cause intergranular fracture. The dimpled appearance of the intergranular facets in the heat-affected zone of the weldments was morphologically identical in every respect to that reported in studies of high-temperature gas bubble embrittlement where the embrittlement is ascribed to intergranular cavity growth. Moreover, further evidence of the role that helium played in the degrading weldability is derived from transmission electron microscopy, where the growth and coalescence of grain boundary helium bubbles in the heat-affected zone of a weldment has been directly observed (Refs. 3, 19).

In welding, the actual driving forces for cavity growth can be found in both the high temperatures and in the stresses that are generated in the heat-affected zone beneath the weld. Thermomechanical modeling of the weld overlays indicates that significant shrinkage stresses, transverse to the weld (parallel to the fusion line) are generated as the weld cools (Ref. 8). For a diffusive cavity growth process, one would expect that those boundaries oriented normal to these shrinkage stresses would be the most susceptible to cracking. The metallographic observations indicate that this was the case, with the great majority of the cracks oriented in this preferred direction. Further, the grain boundary cracks that were most nearly normal to the fusion zone showed the greatest separation, indicating that the shrinkage stresses were greatest in the transverse direction with respect to the weld. Much larger shrinkage stresses created within the HAZ by the deeper penetration stringer bead welds result in significantly more cracking.

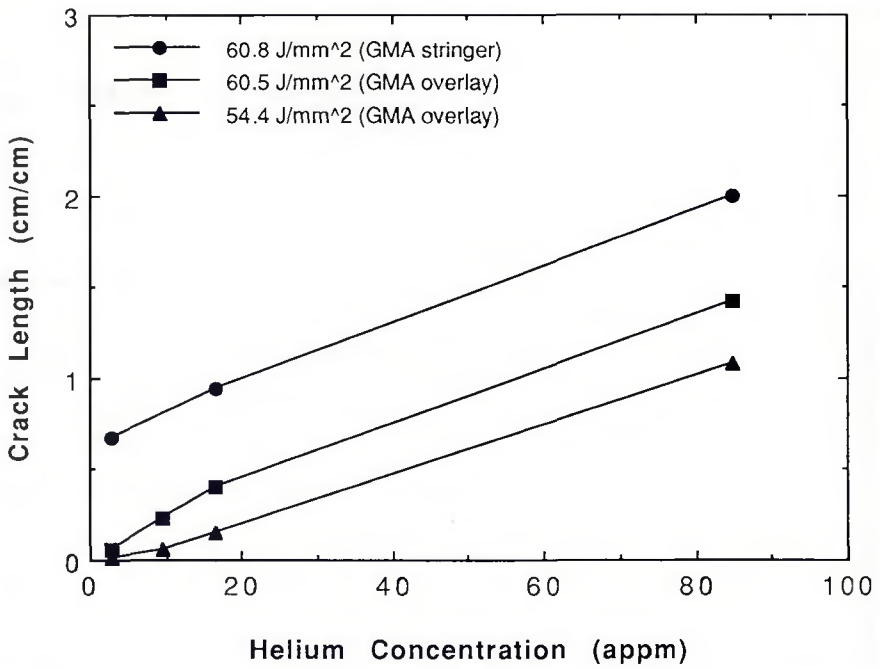


*Fig. 12 — Summary of total crack length (est.) as function of helium concentration. Weld overlays are represented by the solid lines. Stringer weld are represented by the broken line.*

## Conclusions

Metallographic analysis of GMA welds fabricated on helium-bearing 304 stainless steel plates revealed the presence of heat-affected zone cracking and cracking in the fusion zone. The morphology of the cracking suggested that the degradation in weldability resulted from intergranular cavity growth and coalescence via a high-temperature gas bubble embrittlement process. The entrapped helium served only to nucleate a gas bubble microstructure prior to welding.

1) The extent of this damage depended on heat input. Minimizing the heat input, as was done in the overlay welds, significantly reduced all manner of damage.

2) Cracking in conventional, deep-penetration stringer bead welds was much more extensive than in shallow-penetration weld overlays, indicating that the welding process was equally important in determining weldability.

3) The greatest degree of microstructural damage was found in the highest helium content specimen for all welding conditions.

The overlay technique described shows great promise for minimizing the characteristic cracking associated with the welding of helium-bearing materials.

*Acknowledgments*

The authors wish to acknowledge the role of a number of individuals at Westinghouse, Savannah River Co., for their participation in this program. In particular, E. A. Franco-Ferreira is solely responsible for the development of the welding facility and welding processes discussed here. He is also acknowledged for fabricating the welds on the test specimens evaluated in this study. A. K. Birchenall and W. R. Kanne (also WSRC) are also acknowledged for contribution in the development and coordination of the test program.

*References*

1. Maloney, J. P. 1969. *Repair of a Nuclear Reactor Vessel.* E.I. DuPont de Nemours & Co., Savannah River Laboratory, DP-1199.

2. Kanne, W. R. Jr., 1988. Remote reactor repair: GTA weld cracking caused by entrapped helium. *Welding Journal,* 67(8):33–39.

3. Lin, H. T., Goods, S. H., Grossbeck, M. L., and Chin, B. A. 1988. Helium induced degradation in the weldability of an austenitic stainless steel. *Proceedings of the 14th International Conf. on the Effects of Radiation on Materials,* ASTM STP 1046.

4. Louthan, M. R., and Derrick, R. G. 1973. Hydrogen transport in austenitic stainless steels. *Corr. Sci,* 15:565–577.

5. Baskes, M. I. 1983. *Diffuse 83,* Sandia National Laboratories, SAND83-8231.

6. Robinson, S. L. 1987. Tritium and helium effects on plastic deformation of AISI 316 stainless steel. *Mater. Sci and Engr.,* 96:7–16.

7. Goods, S. H. unpublished research.

8. Ortega, A. R. 1990. *A Two-Dimensional Thermal-Mechanical Simulation of a Gas Metal Arc Welding Process.* Sandia National Laboratories, SAND90-8204.

9. Shogan, R. P. Westinghouse Science and Technology Center, Private communication.

10. Hull, D., and Rimmer, D. E. 1959. Growth of grain boundary voids under stress, *Phil. Mag.,* 4:673–687.

11. Raj, R., and Ashby, M. F. 1975. Intergranular fracture at elevated temperatures. *Acta Metall.*, 23:653-666.

12. Chuang, T., and Rice, J. R. 1973. Shape of intergranular creep cracks growing by surface diffusion. *Acta Metall.* 21:1625-1628.

13. Beere, W., and Speight, M. V. 1978. Creep cavitation by vacancy diffusion in plastically deforming solid. *Metall Sci.*, 12:172-176.

14. Edward, G. H., and Ashby, M. F. 1979. Intergranular fracture during power law creep. *Acta Metall.*, 27:1505-1518.

15. Goods, S. H., and Nix, W. D. 1978. Kinetics of cavity growth and creep fracture in Ag-containing implanted grain boundary cavities. *Actal Metall.*, 26:739-752.

16. Nieh. T. G., and Nix, W. D. 1979. A study of intergranular cavity growth in Ag + 0.1% MgO at elevated temperatures. *Acta Metall.*, 27:1097-1104.

17. Stanzl, S. E., Argon, A. S., and Tschegg, E. K. 1983. *Acta Metall.*, 31:833.

18. Mintz, J. M. 1986. Kinetics of stress-induced cavity growth at elevated temperatures. Ph.D. thesis, University of California, Davis, Calif.

19. Lin, H. T., Grossbeck, M. L., and Chin, B. A. Cavity microstructure and kinetics during GTA welding of helium-containing stainless steel. *Trans A.I.M.E.* (A), To be published.

# WRC Bulletin 360
# January 1991

## Stress Indices, Pressure Design and Stress Intensification Factors for Laterals in Piping

**By E. C. Rodabaugh**

The study described in this report was initiated in 1987 by the PVRC Design Division Committee on Piping, Pumps and Valves, under a grant to E. C. Rodabaugh following an informal request from the ASME Boiler and Pressure Vessel Committee, Working Group on Piping (WGPD (SGD) (SC-II) to develop stress indices and stress intensification factors (*i*-factors) for piping system laterals that could be considered by the ASME committee for incorporation into the Code.

In this study, E. C. Rodabaugh considered all available information on lateral connections in concert with existing design guidance for 90-deg branch connections; and has developed compatible design guidance for lateral connections for piping system design. As a corollary bonus, he has also extended the parameter range for the "B" stress indices for 90-deg branch connections from d/D = 0.5 (the present Code limit) to d/D = 1.0. Therefore, this report should be of significant interest to the B31 industrial piping code committees, as well as the ASME Boiler and Pressure Vessel Committee.

Publication of this report was sponsored by the Committee on Piping, Pumps and Valves of the Design Division of the Pressure Vessel Research Council. The price of WRC Bulletin 360 is $30.00 per copy, plus $5.00 for U.S. or $10.00 for overseas postage and handling. Orders should be sent with payment to the Welding Research Council, 345 E. 47th St., Room 1301, New York, NY 10017.

---

# WRC Bulletin 361
# February 1991

This Bulletin contains two reports that compare the French RCC-M Pressure Vessel Code and the U.S. ASME Section III Code on Design of Nuclear Components and Piping Design Rules.

## (1) Improvements on Fatigue Analysis Methods for the Design of Nuclear Components Subjected to the French RCC-M Code

**By J. M. Grandemange, J. Heliot, J. Vagner, A. Morel and C. Faidy**

## (2) Framatome View on the Comparison between Class 1 and Class 2 RCC-M Piping Design Rules

**By C. Heng and J. M. Grandemange**

Publication of this report was sponsored by the Pressure Vessel Research Council of the Welding Research Council. The price of WRC Bulletin 361 is $30.00 per copy, plus $5.00 for U.S. or $10 for overseas postage and handling. Orders should be sent with payment to the Welding Research Council, 345 E. 47th St., Room 1301, New York, NY 10017.